Los Alamos
NATIONAL LABORATORY
EST.1943

LA-UR-15-20757
Approved for public release; distribution is unlimited.

Title: Modeling of Sylgard Adhesive Strength

Author(s): Stevens, Ralph Robert

Intended for: Internal Distribution

Issued: 2015-02-03

Disclaimer:
Los Alamos National Laboratory, an affirmative action/equal opportunity employer,is operated by the Los Alamos National Security, LLC for the National NuclearSecurity Administration of the U.S. Department of Energy under contract DE-AC52-06NA25396. By approving this article, the publisher recognizes that the U.S. Government retains nonexclusive, royalty-free license to publish or reproduce the published form of this contribution, or to allow others to do so, for U.S. Government purposes. Los Alamos National Laboratory requests that the publisher identify this article as work performed under the auspices of the U.S. Departmentof Energy. Los Alamos National Laboratory strongly supports academic freedom and a researcher's right to publish; as an institution, however, the Laboratory does not endorse the viewpoint of a publication or guarantee its technical correctness.

Modeling of Sylgard Adhesive Strength

Ralph Robert Stevens
Los Alamos National Laboratory
January 29, 2015

Introduction

Sylgard is the name of a silicone elastomeric potting material manufactured by Dow Corning Corporation.[1] Although the manufacturer cites its low adhesive strength as a feature of this product, thin layers of Sylgard do in fact have a non-negligible strength, which has been measured in recent tensile and shear debonding tests. The adhesive strength of thin layers of Sylgard potting material can be important in applications in which components having significantly different thermal expansion properties are potted together, and the potted assembly is subjected to temperature changes. The tensile and shear tractions developed on the potted surfaces of the components can cause significant internal stresses, particularly for components made of low-strength materials with a high area-to-volume ratio.

This report is organized as follows: recent Sylgard debonding tests are first briefly summarized, with particular attention to the adhesion between Sylgard and PBX 9501, and also between Sylgard and aluminum. Next, the type of numerical model that will be used to simulate the debonding behavior exhibited in these tests is described. Then the calibration of the debonding model will be illustrated. Finally, the method by which the model parameters are adjusted (scaled) to be applicable to other, non-tested bond thicknesses is summarized, and all parameters of the model (scaled and unscaled) are presented so that other investigators can reproduce all of the simulations described in this report as well as simulations of the application of interest.

1 Summary of Sylgard Bond Strength Tests

A series of mechanical characterization tests have recently been completed in which thin layers of Sylgard potting have been subjected to tensile or shear loads. The details of the Sylgard formulation and preparation, specimen fabrication, and testing

[1] Sylgard is a registered trademark of Dow Corning Corporation.

procedures have been published by Smith [21]. All tests were conducted at room temperature. A short summary of the tests and results that were utilized to calibrate the Sylgard debonding model follows. In many cases the tests were conducted at two or more deformation rates; the results used here those for the lowest available extension rate (typically 0.00008 - 0.0002 in/min) because these rates are most applicable to the intended application of the Sylgard debonding model.

1.1 Shear tests

Two types of specimens were used to measure the shear load-deflection behavior: an Iosipescu specimen and a simple block-on-block lap shear specimen. These specimens are illustrated in Fig. 1. The most important differences in these tests were due to the compliance of the specimen and testing fixtures, and the method of measuring the shear deflection across the bond.

Iosipescu Specimens, Sylgard / Aluminum Bond

In the case of the Iosipescu specimen (also called a "bowtie" specimen), the tested substrate materials included aluminum and PBX 9501. The thickness of the Sylgard bond was nominally 5 mil (0.127 mm). Some of these tests (Sylgard / aluminum specimens only) were conducted using a displacement measurement technique called "digital image correlation" (DIC) that provided an accurate local displacement measurement (where local means directly across the Sylgard bond; unaffected by the compliance of other elements in the load path). The load-deflection results of one of these tests are shown in Fig. 2, which shows both the DIC-measured shear deflection and the crosshead-measured shear deflection. In this measurement, the slope of the loading portion of these two curves is about equal (except at low loads at the beginning of the test), which indicates that the stiffness of the testing apparatus is significantly higher than the stiffness of the Sylgard layer. However, at low loads there appears to be a considerable amount of compliance, possibly due to the fixture[2] that guides the Iosipescu specimen, or to initial clearance or other departure from a "perfect fit" of the Iosipescu specimen in the fixture.

Iosipescu Specimens, Sylgard / PBX 9501 Bond

The measured load-deflection behavior of the Sylgard / PBX 9501 Iosipescu specimens are shown in Fig. 3. Note that the deflection measured in this series of tests is the

[2] The Iosipescu fixture used in this series of tests clamped both ends of the specimen, and included a sliding linear bearing to guide the shearing deformation.

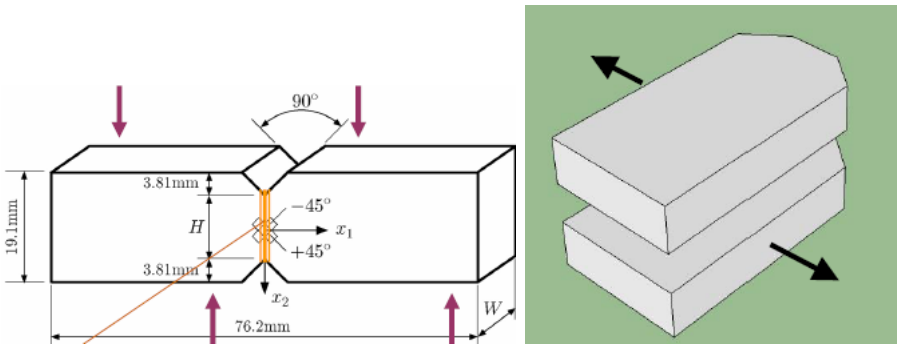

Figure 1: The Iosipescu specimen (left) and the block specimen (right) used in the shear tests. (Figures from Thompson [24] and [25].)

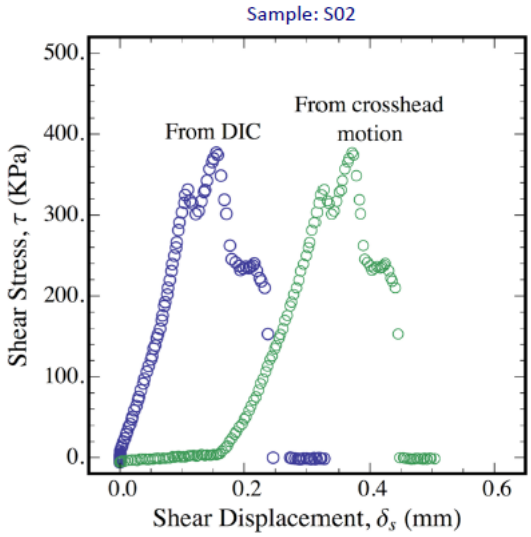

Figure 2: A load-deflection measurement of an aluminum / Sylgard Iosipescu specimen. The shear displacement of the Sylgard layer was measured by an optical method (DIC) and by the crosshead motion of the test machine. (Figure from Liu [15].)

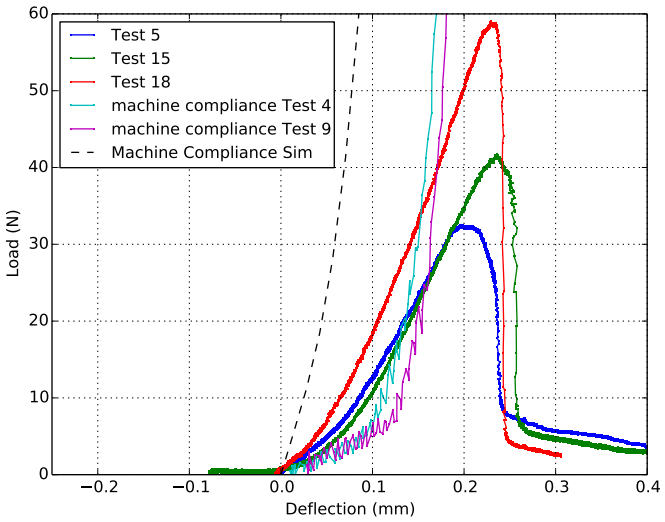

Figure 3: Load-deflection measurements of three PBX 9501 / Sylgard Iosipescu specimens. The shear displacement of the Sylgard layer was measured by the crosshead motion of the test machine only. The tests that used the slowest shear extension rates (0.00008 - 0.0002 in/min) are shown. Machine compliance measurements were also made and are shown in this plot. Note that the measured machine stiffness is not significantly higher than the stiffness of the Sylgard specimens until relatively high force level is achieved.

testing machine's crosshead motion: no local (directly across the bond line) shear deflection was measured. This series of tests used a different Iosipescu specimen holding fixture than the test series described above.[3] The stiffness of the testing apparatus in these tests was measured using a surrogate all-aluminum (no Sylgard) Iosipescu specimen; the load-deflection behavior with this specimen is also shown in the figure. The stiffness of the testing apparatus indicated by the slope of this line is not significantly larger than the stiffness of the Sylgard / PBX 9501 specimens, especially at low force levels. This means that the measured load-deflection behavior is a property of *both* the Sylgard layer and the compliance of the testing apparatus, which makes these results difficult to directly use for calibration of some aspects of the Sylgard debonding model.

[3] The Iosipescu fixture used for the Sylgard / PBX 9501 specimens did not clamp the specimen, but rather contacted it at four points. It is noted that this method of holding the specimen represents an over-determined system (one of the four contact points is not necessary for static equilibrium). To accommodate the fact that the specimens did not "fit perfectly" into the testing apparatus, the test operators in some cases used shims to ensure all four contact points were "tight" at the beginning of the test. This fixture also used a linear bearing to guide the shearing deformation.

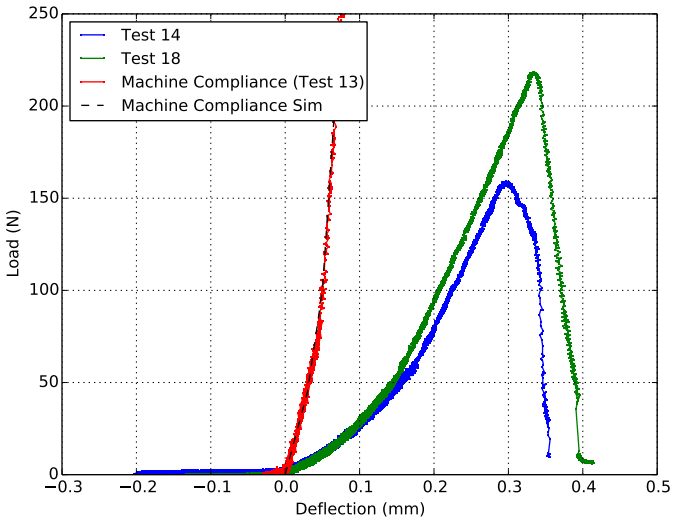

Figure 4: The load-deflection measurements using the PBX 9501 / Sylgard Block specimens. The shear displacement of the Sylgard layer was measured by the crosshead motion of the test apparatus. The tests that used the slow shear extension rate (0.0002 in/min) are shown. Machine compliance was measured and is also shown.

Block Specimens, Sylgard / PBX 9501 Bond

The second shear test series was conducted using the shear-block specimen. The block specimens consisted of two blocks of PBX 9501 bonded together with a 9-mil (0.23 mm) layer of Sylgard. Only the load frame's crosshead displacement measurement was available with these specimens, but this proved to be quite usable because the compliance of the whole system (load frame, fixtures, load cell) was measured, and was significantly stiffer (about 10 times as stiff) than the Sylgard bond itself, even at very low load levels. The load-deflection results from these tests are shown in Fig. 4, which shows the results of two tests conducted at the lowest tested loading rate (0.0002 in/min). Tests conducted at higher loading rates indicated that there does appear to be some dependence of peak load on the rate of deformation.

1.2 Tension Tests

Two types of butt joint specimens were used to measure the tensile debonding strength of Sylgard. For the tests of Sylgard bonded to aluminum, a simple cylindrical specimen was used, which consisted of aluminum substrates joined by a thin (5 mil = 0.127 mm nominal thickness) layer of Sylgard. For these specimens, the axial extension of the bond was measured using a scanning laser extensometer. Plots of the

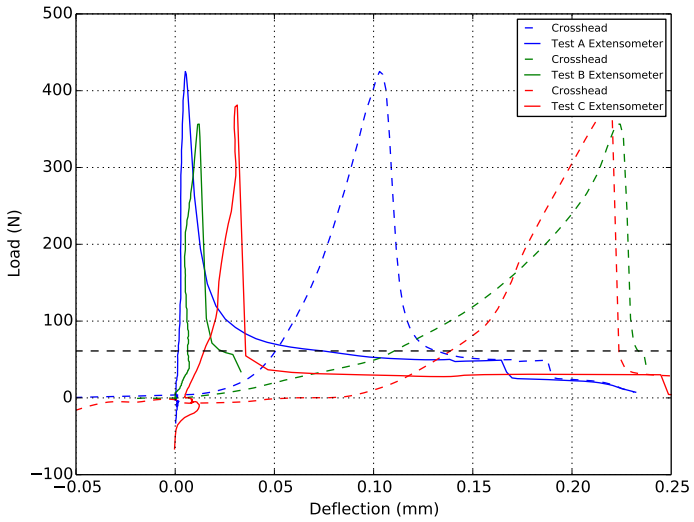

Figure 5: The tensile load-deflection measurements of an aluminum / Sylgard specimen. The axial extension of the Sylgard layer was measured by an extensometer and by the crosshead motion of the test apparatus.

force plotted against the extension measured by the laser extensometer, as well as the extension measured by the crosshead, are shown in Fig. 5. These results will be considerd in detail in Section 4.

For all tensile tests of Sylgard bonded to PBX 9501, a "dogbone" specimen was used. This is a standard specimen for tensile tests of HE. For these Sylgard bond tests, the specimen was simply cut in half, then bonded back together with a 5 mil (0.127 mm) thick Sylgard bond. Only the testing machine's crosshead deflection was measured with these specimens. The results of these Sylgard / PBX 9501 debonding tests are shown in Fig. 6. These load-deflection results are strongly affected by the compliance of the testing apparatus, both on the front slope and for the post-peak behavior. Although the fixturing compliance was not measured in this series of tests, a good estimate was available from previous PBX 9501 dogbone tests of "whole" specimens (PBX 9501 specimens with no Sylgard bond). A stiffness of 350 N/mm was determined, based on a test[4] conducted at similar rate and temperature. This stiffness is very close to the stiffness exhibited by the specimens in Fig. 6, confirming that nearly all of the front slope compliance is due to the HE part of the specimen, not due to the thin Sylgard layer.

[4] This stiffness estimate was based on specimen 083109c, which was tested as part of 2009 Enhanced Surveillance Campaign UH baseline study.

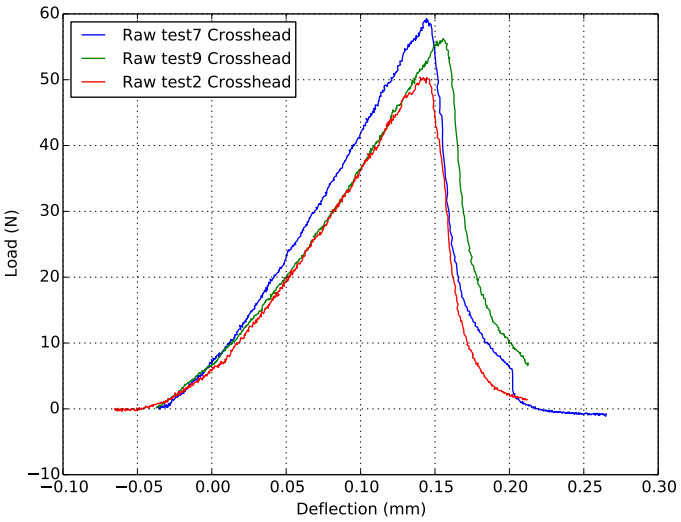

Figure 6: The tensile load-deflection measurements from the Sylgard / PBX 9501 dogbone specimens. The axial extension of the Sylgard layer was measured by the crosshead motion of the test apparatus. The slow extension rate tests are shown (0.0002 in/min).

2 Modeling Assumptions and Cohesive Zone Models

A cohesive zone model in the form of a surface-based contact interaction was used to model the Sylgard debonding process. In this approach, the interface between the Sylgard and the adjacent component (to which the Sylgard is initially bonded) is modeled using a contact interaction that enforces a no slip, no separation condition (actually a stiff elastic relation similar to a contact penalty stiffness) until a damage initiation criterion is reached. At this point, the stiffness of the tied contact interaction is gradually degraded, following a damage evolution rule, and the two materials are allowed to separate along the previously tied interface, effectively creating new free surfaces. This debonding model treats the decohesion of the bond as a property of the interface: the Sylgard material itself and the neighboring component are both modeled with finite elements and using material models that "know nothing" about failure and have no softening behavior.[5] The Sylgard material model is described in

[5] A similar approach uses so-called cohesive elements rather than a cohesive contact interaction. In this approach, special elements are used to model the Sylgard (rather than the ordinary finite elements and material model used by the cohesive contact approach). After a damage initiation criterion has been reached, the stiffness of these cohesive elements is progressively degraded following a similar damage evolution rule. No new free surface is created by the debonding process: the cohesive elements remain tied to the adjacent components, and the debonding process is modeled as a behavior of the bulk material (that is, the behavior of the cohesive elements), not of the fracture surface (defined by the behavior of the contact interaction).

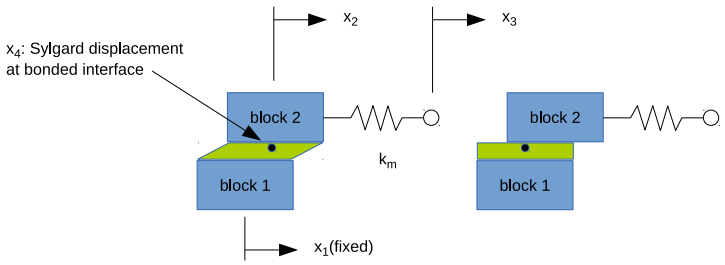

Figure 7: Schematic diagram of the shear test. The Sylgard layer (green) is initially bonded to both blocks. As the test machine's crosshead displacement (x_3) increases (left figure), the Sylgard bond deforms in shear ($x_4 = x_2$) and the test apparatus (represented by spring k_m) also deforms. After complete debonding (right figure), the free surface of the Sylgard layer returns to a unstressed configuration ($x_4 = x_1$). Note that all debonding is assumed to occur on only one interface.

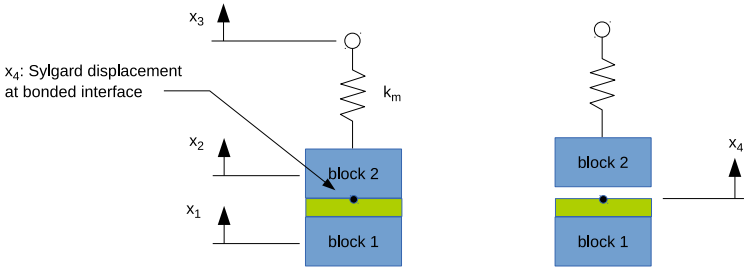

Figure 8: Schematic diagram of the tension test. The elements of the test and the displacments x_1, x_2, x_3, and x_4 have the same meaning as those shown for the shear test in Fig. 7.

Appendix 1. The cohesive zone model and its implementation in the analysis code is described in detail below, following a brief description of other aspects of the model.

A schematic diagram of the shear test is shown in Fig. 7, and for the tension test (using the same terms) in Fig. 8. The stiffness and displacement quantities shown in this diagram are referred to throughout this report.

It is assumed that debonding occurs entirely on one side of the Sylgard interface. The other interface (the other side of the thin Sylgard layer) is typically tied to the surface of the adjacent part ("block 1"), with no debonding possible. This modeling assumption was investigated and described in Appendix 2.

The term stiffness (denoted k) refers to the force required to produce a given amount of deflection in an elastic system; it is the slope of a load vs. deflection response. The stiffness can be normalized by the area of an interface; this quantity is denoted K_n or K_s (stiffness per unit area in the direction normal to a thin layer, or in an in-plane direction, respectively). These quantities should not be confused with the

elastic bulk modulus, denoted K. Equivalently, these stiffness per unit area quantities can be thought of as the slope of a stress vs. deflection response, where (typically) this is a nominal stress (for example, the measured load normalized by the original bonded area).

The stiffness of an adhesive layer is dependent on material properties and the thickness of the layer, as well as on the cross-sectional area of the specimen. If the stiffness is proportional to the cross-sectional area, then the stiffness per unit area, K_n, is a meaningful way to characterize the load-deflection behavior of the bond, in a way that eliminates the dependence on the size of the bond. So, for example, K_n and K_s are meaningful quantities when comparing different diameter specimens with the same bond thickness, when the displacement is measured locally across the bond thickness. However, if the measured displacement includes significant contribution from other deformable parts of the test apparatus, normalizing the calculated stiffness by this one particular factor (area) is not meaningful.

In a load-deflection test, the load is transmitted through many parts of the measurement apparatus in addition to the specimen itself (for example, the specimen grips or holding fixture, the load cell, and the testing machine's frame). In thin-layer adhesive bond tests, the portion of the specimen that serves as the "rigid" substrate (to which the adhesive layer is bonded) must also be considered part of the testing apparatus. Each of these parts has a finite stiffness, and the series-combination of these stiffnesses may not be large in comparison to the stiffness of the specimen (layer of adhesive) itself. This is especially true at low load levels due to contact seating and backlash effects in the test apparatus. The net stiffness of the entire load-deflection measurment system (all elements other than the adhesive layer under test) is called the machine stiffness, k_m (but often referred to by its reciprocal, the machine compliance). In some of the Sylgard debonding tests the machine stiffness was measured. It is noted that the machine stiffness strongly affects the control and stability of a test if the specimen exhibits a softening behavior.

A type of instability is encountered in some of the Sylgard debonding tests, and in the corresponding simulations. An unstable situation exists when the elastic deformation developed in the test machine, fixturing, and specimen at peak load exceeds the separation distance of the debonding traction-separation law. In this case, there is no continuous path of static equilibrium states during the period of time between the moment of peak load and the state of complete failure (zero load-carrying capability), during which the Sylgard bond is in a softening regime. This situation is evidenced by a very steep back slope (unloading) in the crosshead-measured load-deflection behavior. It is also evident in plots of force vs. time: the force drops from its peak value to a small level suddenly. This instability is most obvious in tests with relatively high compliance (low stiffness): this was especially true in all tests using the Iosipescu specimens.

To enable a static analysis of tests that included unstable behavior, a small amount of damping was added to the model of the test. Three different techniques were considered: using a discrete damper, using contact damping in the cohesive contact interaction definition, and using the "dynamic stabilization" feature of the analysis code's cohesive contact capability. It was found that the contact damping approach was robust and offered more options to control how the damping was applied (for example, separate damping levels could be applied for normal and tangential motions). In all cases, the total force carried by the damping was compared to the (real) applied force in the tests to ensure that this damping remained a small fraction of the total.

2.1 Cohesive Zone Models in Structural Analysis

The cohesive zone model (CZM) approach is a well-established method to model interfacial fracture. The CZM approach assumes that a cohesive damage zone (a region of degraded cohesive strength) develops over a finite region of material (called the fracture process zone). Cohesive damage zone models relate interfacial tractions to separation displacements at an interface, thereby linking the microstructural failure mechanism to the continuum fields governing bulk deformations. A CZM is characterized by the properties of the bulk material, the crack initiation condition, and the crack evolution function. Cohesive zone models have been used to model many different types of separation processes such as void growth and coalescence, fiber bridging, atomic separation, and separation of adhesive layers. Traction and separation in cohesive zone models are work conjugate, as stress and strain are strain energy conjugate. Strain in the cohesive zone is irrelevant.

In the structural analysis code Abaqus [1], surface-based adhesive behavior is defined as a property of a pair of contacting surfaces. It is used to model the adhesive failure (fracture) directly in terms of surface tractions and surface-to-surface separation distance. A linear elastic traction-separation behavior of the interface (*not* of the bulk material) is assumed prior to damage. Failure of the adhesive bond is treated as a progressive degradation of the pre-damage adhesive interfacial stiffness. After failure, the two surfaces continue to interact without any adhesive attraction (that is, they may not penetrate each other).

The initial (undamaged) traction-separaton model assumes a linear relationship between the nominal stress traction vector and the node-to-surface separations. Terms used to describe the behavior of this model are illustrated in Fig. 9. In the uncoupled form used here, these relations are:

$$\tau_n = K_n \, \delta_n \tag{1}$$

$$\tau_s = K_s \, \delta_s \tag{2}$$

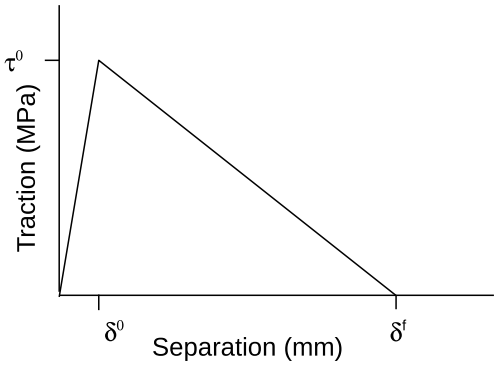

Figure 9: The traction-separation rule defining interface debonding. Using the terms from Fig. 7, the separation distance (at any time during the debonding process) is $\delta = x_2 - x_4$.

where τ is a component of the stress traction in the normal or shear direction, δ is a component of the separation distance (defined for each slave node relative to its master surface), and K_n and K_s are the stiffness per unit area terms for the undamaged elastic response. Note that when this adhesive layer is modeled with finite elements,[6] these stiffness terms are included in series with the stiffness of the adhesive layer itself, and the separation distance is the separation between the two initially-bonded surfaces:

$$\delta = x_2 - x_4 \tag{3}$$

where x_2 and x_4 are defined in Fig. 7 and Fig. 8. The surface-to-surface interfacial stiffness terms K_n and K_s can be used to represent a reduced stiffness for tensile behavior that a coarse mesh may be unable to accurately capture. The choice of these terms will be discussed in the next section. Also, note that this model of a linear relation between tractions and separations applies only during adhesive separation; in compression, the "ordinary" contact interactions apply.

The linear relation between the applied tractions and the opening displacements defined by eqs. 1 and 2 is maintained until a damage initiation criterion is reached. In the form of the model used here, the damage initiation criterion ("maximum stress criterion") is reached when either the normal traction τ_n reaches the normal traction limit, τ_n^0, or when the shear traction τ_s reaches the shear traction limit τ_s^0 (the zero superscript refers to the point at which damage initially begins to evolve). This debonding initiation in a mixed loading (with both tension and shear) is reasonable,

[6] The adhesive layer may or may not be modeled explicitely with finite elements. When the thickness of this layer is negligible, it may be omitted (that is, the adhesive layer is not modeled with any finite elements at all); in this case the linear K_n and K_s terms must represent the entire stiffness of the layer, and a geometric approximation must be made to the adjacent components.

but it is noted that this is in fact a modeling simplification; it is not based on any mixed-mode debonding test results.

The progressive failure of the adhesive bond (the behavior after the damage initiation criterion has been reached) is modeled by scaling the elastic tensile and shear stiffness terms (K_n and K_s) by a factor, $(1 - D)$, where D evolves from 0 (undamaged state, effective separation distance $\delta_m = \delta_m^0$) to 1 (completely failed state, effective separation distance $\delta_m = \delta_m^f$) according to a damage evolution criterion. This damage evolution criterion defines the rate at which the damage variable D grows and its dependence on the effective separation distance:

$$\delta_m = \sqrt{\delta_n^2 + \delta_s^2 + \delta_t^2} \tag{4}$$

The single damage variable D is used to scale both the tensile and shear undamaged stiffness values. It is noted, however, that some investigators [6] have reported no damage-like effects on the shear response caused by previous tensile loading history that did produce a degradation of tensile stiffness.

3 Calibration of Debond Model

3.1 Shear Debonding

Front slope stiffness

The simulations of the Iosipescu and block shear specimen tests described in Appendix 1 indicate that the elastic material model can reproduce the undamaged shear response of the bulk Sylgard layer observed in the tests. This is true even with a very coarse mesh, even with a single element through the Sylgard layer thickness. This fact indicates that a "high" interfacial shear stiffness term, K_s, is appropriate for the shear traction-separation rule. This is the default behavior for the model: unless specified otherwise, the analysis code uses a large K_s term based on a penalty contact stiffness behavior.[7] However, it has been found that relying on the default K_s stiffness term provided by Abaqus leads to poor performance (numerous time step cutbacks) of the cohesive contact interface. A lower K_s value permits Abaqus to take larger time steps as the shear traction is reduced at the beginning of the damaging portion of the response. It is found that a value of K_s that is on the order of 100 times the shear stiffness of the Sylgard layer itself is high enough to allow only a

[7] The penalty contact stiffness calculated by the analysis code is chosen to be high enough to ensure that contact overclosure (penetration in compression, slip in shear) is negligible compared to the elastic deformation of the elements adjacent (on both sides) to the contact interface.

neglible interfacial shear displacement at the peak shear traction, while still greatly reducing the number of time steps required to simulate the debonding process. A recommended value is:

$$K_s = 100(G/t) \tag{5}$$

where G is the shear modulus of Sylgard and t is the bond thickness. It was verified that the simulation results were not sensitive to the particular value of K_s used in the simulation, until K_s values much lower[8] than this were considered.

Damage Initiation and Damage Evolution

The peak bond shear traction τ_s was measured in the PBX 9501 / Sylgard block shear specimens and the PBX 9501 / Sylgard Iosipescu specimens. Because a slow loading rate was most relevant in the application of interest, the low-rate test data was used for calibration. These test results were shown in Fig. 3 (Iosipescu specimens) and Fig. 4 (Block specimens). An average of the peak nominal shear stress (load divided by original bonded area) from the two low-rate PBX 9501 tests was used. This average value was 0.26 MPa for the block specimens (bond thickness 9 mil), and 0.30 MPa for the Iosipescu specimens (bond thickness 5 mil). A higher bond strength is expected for a smaller bond thickness (see next section), but it is noted that there was significant scatter in the test results (particularly in the tests using the Iosipescu specimens).

The fully-debonded separation distance δ_s^f was based on the PBX 9501 / Sylgard block specimens only: the Iosipescu specimens were not used for this purpose because the low stiffness (high compliance) of the test apparatus (which includes the Iosipescu specimen and loading fixture) combined with the compliance of the Sylgard layer itself (before damage) produced a shear displacement at peak force that was greater than the δ_s^f of the bond. A consequence of this was that the measured load-deflection curves for the Iosipescu specimens tended to drop from the peak load to zero "suddenly." This is evidenced by the very steep back-slope in the load-deflection plots (Figs. 3 and 4), and by the sudden change in force in the force vs. time plot (not shown here). In contrast, the back slope of the load-deflection curves for the block specimens was resolved: the back slope is not vertical, but rather there are many load and extension measurement samples during the softening response as the applied load dropped from maximum to zero. This difference in measured post-peak behavior is thought to be due to the higher peak load in the block shear specimen (due to block specimen's greater size), which puts the testing apparatus further away from the highly-compliant, nearly-unloaded portion of the initial response. Also, the block specimen and fixturing is inherently stiffer than the Iosipescu specimen and its fixtur-

[8] The added compliance was not noticeable until K_s values less than $10(G/t)$ were used.

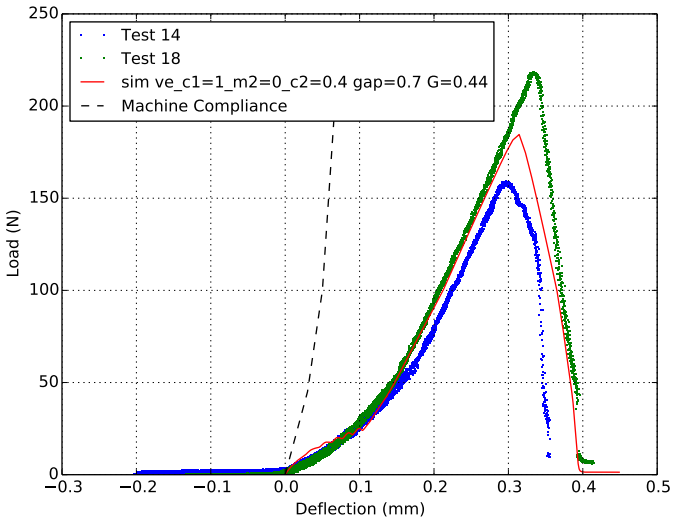

Figure 10: Comparison of the two low-rate shear block specimen tests (Sylgard / PBX 9501), and the simulation of these tests. The measured machine compliance is also shown.

ing (which includes a linear bearing); this is especially true for the PBX 9501/Sylgard specimens.[9]

The fully-debonded separation distance δ_s^f was estimated by careful inspection of the measured load-deflection behavior of the block shear specimens, and iterative simulations of these tests using trial values. In these simulations, it was essential to have a reasonably accurate prediction of the undamaged portion of the load-deflection behavior. As described previously, this required a good model for the bulk elastic behavior, and the inclusion of a nonlinear spring to represent the machine compliance. The shear block test data and the results of the simulation of these tests are shown in Fig. 10.

A simulation of the Iosipescu specimen (Sylgard / PBX 9501) results is shown in Fig. 11. Note that these tests were not used to calibrate the fully-debonded separation distance δ_s^f, as mentioned above, due to the unstable softening response. Also, for this reason, contact damping was required to carry-out the simulation past the peak load. A significant "toe correction" had to be applied the measured machine stiffness behavior because, as illustrated in Fig. 3, at low loads, the apparent deflection of the machine was greater than the measured deflection of the Sylgard / PBX 9501

[9] Machine compliance measurements were made using an all-aluminum Iosipescu specimen (that is, with no Sylgard bond layer). Considerable variation in these machine compliance measurements was observed at low force levels. No machine compliance measurement was made using an all PBX 9501 specimen. The compliance due to deformation of the PBX 9501 may be quite significant in these test results.

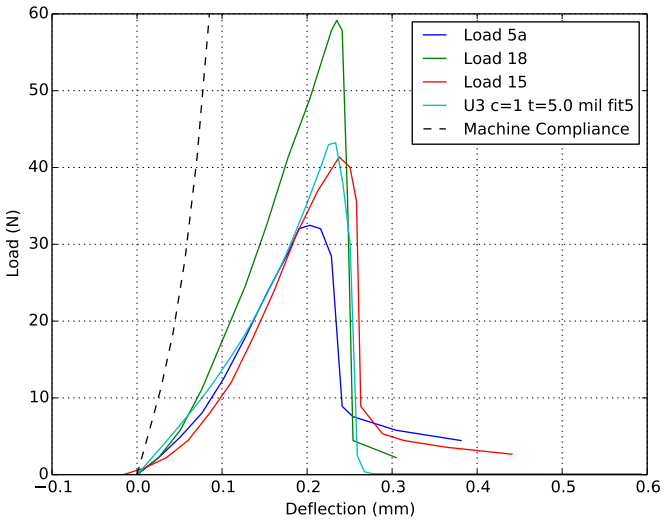

Figure 11: Comparison of the low-rate shear Iosipescu specimen tests (Sylgard / PBX 9501), and the simulation of these tests. These tests exhibited a sudden drop in load with a nearly-vertical back slope, indicating an unstable response. The machine compliance curve (dashed line) was used in this simulation.

specimen (an impossibility, possibly due to non-repeatability in the Iosipescu test set-up).

The two Sylgard / aluminum Iosipescu specimens that were tested using the optical shear displacement measurement technique were also not used to characterize the back slope of the load deflection behavior. Although the shear displacement measurement was unaffected by the compliance of other elements of the test apparatus, the tested configuration itself was identical to the other Iosipescu tests, and the post-peak load-deflection exhibited the same sudden drop in force indicating a statically-unstable situation described previously. It is also noted that these two tests produced a post-peak behavior that was quite different than the post-peak behavior of all of the other Sylgard / aluminum Iosipescu specimens.

3.2 Tensile Debonding Model

Front-Slope Behavior

The tensile load-deflection behavior of thin layers of elastomers is quite difficult to measure because the extension of the layer is very small. It is widely recognized that the effective stiffness of the thin layer is significantly higher than the value that would be obtained for a uniform, uniaxial state of stress (AE/t), due to the

high triaxiality caused by the confinement (restriction of radial strain) of the elastic layer. Simulating the state of stress and strain in the elastomer is certainly possible, but requires a relatively fine mesh (especially near free surfaces) and the use of some special modeling techniques such as hybrid finite elements that uncouple the pressure-volume response from the deviatoric response.

However, the assumptions that the bulk elastomer remains a homogeneous layer of material and that the elastomer and the adjacent substrates remain perfectly adhered to each other break down surprisingly early in the case of "soft" (low shear modulus) elastomers, such as Sylgard, subjected to hydrostatic tension. Some researchers have found methods of imaging thin layers of soft elastomers under tension, and find that small cavities (voids) can nucleate in the bulk material and at the interfaces ([23], [18], [14], [3], [10], [27]). In adhesive strength tests, these cavities are observed well before the peak loads have been reached. The images of the thin layers under tensile applied stress reveal the initial shape and distribution of the cavities as well as the subsequent elongation and coalescence as the separation increases. These images are very helpful in understanding the morphology and bond behavior during the debonding process.

As a part of the Sylgard debonding test series, one set of tests was conducted that used a high-resolution laser extensometer to measure the opening displacement across a thin (nominally 5-mil) layer of Sylgard bonded to aluminum substrates. The load-displacement behavior measured in these tests was shown in Fig. 5. It is interesting to compare the front-slope load deflection behavior exhibited in these tests[10] to the stiffness that is predicted by elastic theory and by finite element simulations. The calculated tensile stiffness (estimated by several methods) and measured tensile stiffness of the thin layer of Sylgard are shown in Table 1. When the compressibility of Sylgard is ignored (effectively treating the bulk modulus as infinite), the stiffness is greatly overpredicted. When the compressibility is included but the layer is treated as fully confined (restrained from radial displacement at the outer edge of the cylindrical specimen), the stiffness is governed only by the pressure-volume relation and the stiffness is simply AK/t.[11] The analytic and finite element predictions of the compressible response with a free surface are not too much different than the compressible, fully-confined solution, which illustrates that the diameter to thickness ratio of this specimen is high enough to make the free surface nearly irrelevant. But all of these approximations are much greater than the stiffness that is measured in the Sylgard debonding tests.

[10] The stiffness values for the tests were calculated as the average stiffness from the unstressed state to the peak stress state ($k = F_{peak}/d_{peak}$, where F_{peak} and d_{peak} are the peak values of load and extension measured in the tests).

[11] This case is not hypothetical: it is the solution that is obtained when using a very coarse mesh consisting of a single linear element through the thickness of the Sylgard layer. In this case the radial displacement is fully restrained (at both substrate interfaces and on the free edge).

Table 1: Comparison of Tensile Stiffness of a Thin Layer of Sylgard

Analytical Approximations	**Stiffness**
Incompressible, homogeneous, elastic response, Gent [9]	k = 9.67e6 N/mm
Compressible, fully confined (no radial deformation at edge, k=AK/t)	k = 4.02e6 N/mm
Compressible, homogeneous elastic response, Shull [20]	k = 3.14e6 N/mm
Compressible, homogeneous elastic response, finite element simulation (coarse mesh: 1 linear element through layer thickness; Neo-Hookean hyperelastic model)	k = 4.16e6 N/mm
Compressible, homogeneous elastic response, finite element simulation (fully-resolved mesh; Neo-Hookean hyperelastic model)	k = 2.48e6 N/mm
Test A	k = 82,800 N/mm
Test B	k = 29,500 N/mm
Test C	k = 12,200 N/mm

Geometry: cylindrical specimen, D=31.75 mm, t = 0.2388 mm
Sylgard elastic model: $G_0 = 0.44$ MPa, $K_0 = 1{,}214$ MPa
Rigid substrates, no separation or slip at interfaces

This discrepancy between the theoretical stiffness of a thin elastic layer and the measured stiffness has been described by Lindner [14]. Using a "tack probe" apparatus, Lindner measured the compliance of thin layers (D/t = 60) of an acrylic adhesive (which has elastic properties similar to Sylgard), and also calculated a theoretical compliance based on an analytical approximation by Shull [20]. The theoretical stiffness was more than an order of magnitude greater than the measured stiffness. The compliance measurement was made at stress levels of approximately one-half of the peak (debonding) stress. Lindner speculates that this discrepancy may be caused by the boundary condition at the interface between the adhesive and the substrate - that is, a deviation from a perfect (spatially continuous) adhesive contact over the entire bonded surface area. Dorfmann [6] also observed a progressive decrease in tensile stiffness of a thin layer of an elastomer. This decrease in tensile stiffness was attributed to the formation of cavities (voids) in the elastomer. Dorfmann found that the damage did not affect the shear or compression response, but permanently affected the tensile response. The onset of the damage was evident at stress levels of roughly one-half of the peak (failure) stress level. Finally, it is noted that, despite best efforts (such as using a vacuum degasser after mixing the Sylgard components), the Sylgard bonds produced in the tests described here sometimes contained visible bubbles, presumably due to air entrained during the potting process. Such bubbles have also been reported in other Sylgard potting applications.

For the purposes of the Sylgard debonding model, an important observation is that the adhesive separation δ_n^0 associated with the peak traction τ_n is small compared to the separation at complete failure δ_n^f:

$$\delta_n = \frac{\tau_n}{K_n} \ll \delta_n^f \tag{6}$$

For this reason, the area under the traction-separation curve (which is equal to the work of adhesion) is only weakly affected by the specific value of K_n used. Simulations conducted with a range of interfacial stiffness values (K_n) demonstrated that this stiffness term does not have a significant effect on the failure load or the load-deflection behavior during damage evolution (after the peak force has been reached), but does influence the solution efficiency (number of time step cutbacks), for the same reasons described above for the shear front slope stiffness term K_s. This observation is also discussed in [26]. With these considerations taken into account, a front slope stiffness value of $K_n = 105\ N/mm^3$ (or MPa/mm), which was estimated from the Sylgard / aluminum specimen deemed to be the best measurement,[12] was taken as representative for all Sylgard bonds (of the same bond thickness).

[12] The front-slope stiffness for Test A, shown in Table 1, was used. A stiffness per unit area of 105 MPa/mm was obtained from the measured stiffness divided by the area of the bond.

Given that this tensile front-slope stiffness value was much smaller than the value expected for a homogeneous elastic response, the need for a fine mesh resolution (in the through-thickness direction) was removed. That is, the compliance for normal-direction load-deflection behavior was controlled by the K_n value, *not* by the finite element mesh and material model which simulate the homogeneous bulk Sylgard response. This fact permitted the use of very coarse finite element meshes, including a single finite element through the thickness of the potting layer.

Damage Initiation and Damage Evolution

The peak tensile traction was taken directly from the average of the tensile dogbone specimen tests, which were shown in Fig. 6. As with the shear test data, some apparent rate dependence was observed. The tests with the lowest loading rate were used for this model because they were closest to the the load rates in the application of interest.

The separation at failure δ_n^f was determined by inspection of the load-deflection behavior of the Sylgard / aluminum specimens, as these tests included the local across-the-bond extension measurement. The δ_n^f was confirmed by simulations of these tests (shown in Fig. 12) and also by simulations of the dogbone Sylgard / PBX 9501 tests (shown in Fig. 13). The direct extensometer measurement of the bond extension (for the Sylgard / aluminum specimen) exhibited a rapid initial softening behavior (rapid fall-off in load after the peak load was reached), but also exhibited a long "tail": the load vs. separation curve appeared to be more of an exponential decay than a linear drop-off. The load-deflection behavior of the tensile dogbone PBX 9501 specimens (based only on a crosshead extension measurement) suggested a somewhat larger total δ_n^f value and also an exponential decay. The nominal bond thickness was the same for the Sylgard/aluminum and Sylgard/PBX 9501 tests, so differences in debonding behavior are due to the substrate material only, perhaps due to differences in surface roughness of the substrate materials.

An exponential damage evolution rule was used in these simulations to emulate the observed post-peak behavior. Use of this feature allowed a better representation of the area under the traction-separation law, while maintaining the separation at failure that was measured in the tests. The rate of fall-off of the traction with increasing separation is controlled by a parameter α. A value of $\alpha = 8$ was used in the simulation results shown in Fig. 12 and 13. It is noted that using higher values of α resulted in more difficult convergence (requiring smaller time steps). The agreement between the measured and simulated softening behavior is poor, but the total area under the curve, which is the work of adhesion, is roughly the same.

There are many articles in the literature that describe the use of CZM models to simulate the behavior of adhesive bonds under hydrostatic tensile loading. Several articles that have been especially useful include [17], [10], [22], and [26].

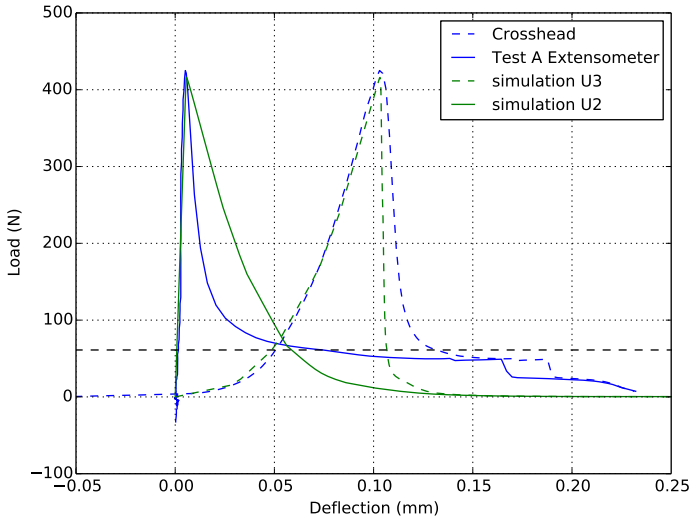

Figure 12: Comparison of the load-extension response of the Sylgard / Aluminum cylinder specimen (Test A). Both the local (across-the-bond) extension measurement and the crosshead extension measurement are shown. The simulation used the crosshead load-deflection measurement as an estimate of the machine stiffness.

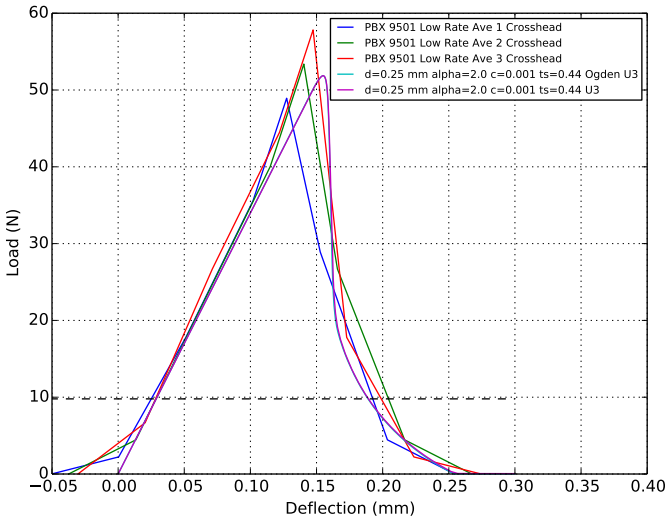

Figure 13: Comparison of the load-extension response of the Sylgard / PBX 9501 dogbone specimens. Only the crosshead deflection was available in this test. The machine compliance measured in an all-PBX 9501 specimen was included in the simulation.

4 Scaling of Debond Model Parameters

The Sylgard debonding tests were carried out using several different substrate materials, but all specimens had a nominal bond thickness of 5 mil (0.127 mm) or, in the case of the shear block specimens, 9 mil (0.229 mm). In the application of interest, the Sylgard bond thickness is 20 mil (0.5 mm). This difference between what was tested and what is used in practice required that some of the traction-separation parameters be scaled. This is a typical problem in modeling and testing adhesive joints, and has been studied by many investigators (for example, Afendi [2]). The basis for scaling the debond model parameters are summarized here, and all parameters (scaled and unscaled) are presented so that other investigators can reproduce all of the simulations described in this report as well as simulations of their application of interest.

The scaling used here follows the investigations described by Chung [4], who investigated the dependence of the pull-off stress required to separate a rigid stud from a thin layer of a soft elastomer, where the diameter of the rigid stud is much greater than the thickness of the elastic layer. Chung developed the general scaling rules from a fracture mechanics basis, and conducted a series of measurements using a tack probe apparatus to confirm his results. The dependence of the average pull-off stress σ_c on the bond thickness t was found to follow the form:

$$\sigma_c \sim \sqrt{\frac{WE}{t}} \tag{7}$$

where W is the work of adhesion and E is the elastomer's Young's modulus. This relationship comes from consideration of the elastic energy associated with the through-thickness extension of the elastomer, taking into account the hydrostatic stress state in the thin layer and the formation of cavities at the interface between the elastomer and the substrate. When W and E are held constant, this relation implies a $1/\sqrt{t}$ relationship between the pull-off stress and bond thickness. Chung conducted a series of experiments to confirm this result, using a soft PDMS elastomer and varying both the thickness and the elastic modulus of the layer. His results indicated a linear relation between the pull-off stress σ_c and the quantity $(E/t)^{1/2}$, confirming the form of the relationship expressed by eq. 7 and implying a constant work of adhesion W.

The work of adhesion in a linear traction-separation model is

$$W = \frac{1}{2}\tau^0\delta^f \tag{8}$$

Holding the work of adhesion constant implies that the separation at failure, δ^f, increases in inverse proportion to the peak traction at initiation of damage, τ^0. So, for example, a specimen with a bond thickness of 20 mil would be expected to exhibit half the peak pull-off stress of a specimen with a bond thickness of 5 mil (eq. 7), and would be also be expected to have twice the separation at failure compared to the 5-mil bond (eq. 8).

The bond thickness scaling form for the front slope stiffness per unit area quantities, K_n and K_s, were also based on a result from Chung. The opening stiffness of a thin layer was determined to be proportional to the area of the bond and inversely proportional to the thickness of the bond:

$$k \sim \frac{a^2 E}{t} \tag{9}$$

where k is the bond stiffness and a is the radius of the (cicular) bond; the stiffness per unit area K_n is this stiffness k divided by the area of the bond.

The tensile front-slope stiffness measurements were described in section 2. The value of K_n measured in these tests was approximately 105 MPa/mm for a tension specimen with a bond thickness of 9.4 mil. As discussed in section 5, the Sylgard mesh and constitutive model are *not* capable of reproducing the observed front slope opening stiffness. This front slope behavior is dominated by interfacial cavity nucleation and growth as the applied traction approaches the bond's peak traction limit (τ_n^o). The finite element mesh and constitutive model can only simulate the homogeneous elastic response, and therefore give an effective stiffness that is much larger than the stiffness observed in the Sylgard debonding tests. Instead, the model relies on the cohesive contact's K_n value to simulate the much lower opening stiffness that is observed in the tensile debonding tests.

Using the scaling relation above, the aluminum / Sylgard specimen with the 9.4 mil bond thickness that exhibited a K_n value of 105 MPa/mm would be expected to have an opening stiffness K_n of 49.3 MPa/mm if its bond thickness were 20 mil. To put these values in perspective, both of these stiffness values result in very small opening displacements. For the tested specimen, at the peak normal traction level, $\tau_n = 0.56$ MPa, the displacement δ_n^0 corresponding to K_n of 105 MPa/mm is 0.005 mm (0.2 mil). Likewise, if that specimen had a bond thickness of 20 mil (0.5 mm), the δ_n^0 resulting from its expected peak normal traction ($\tau_n = 0.28$ MPa) and front slope stiffness ($K_n = 49.3$ MPa/mm) is 0.006 mm (0.2 mil). Both of these opening displacements are small compared to the bond thickness, and compared to the bond separation at failure δ_n^f.

In the case of the shear front slope stiffness, the Sylgard constitutive model and the Sygard finite elements are able to reproduce the observed shearing stiffness. So in

Table 2: Calibrated Debond Model Parameters, from All Test Specimens

	Sylgard to Aluminum	**Sylgard to PBX 9501**
Shear, Iosipescu Specimen, t = 5 mil (note 1):		
τ_s	0.35 MPa	0.30 MPa
δ_s^f	(note 2)	(note 2)
Shear, Block Specimen, t = 9 mil:		
K_s		(note 3)
τ_s	-	0.26 MPa
δ_s^f	-	0.30 mm
Tension, Cylinder Specimen, t = 9.4 mil:		
K_n	105 MPa/mm	-
τ_n	0.56 MPa	-
δ_n^f	0.20 mm	-
Tension, Dogbone Specimen, t = 5 mil:		
τ_n	-	0.44 MPa
δ_n^f	-	0.25 mm
1) Nominal specimen bond thickness		
2) Unstable test response		
3) K_s = 192 MPa/mm recommended; see text.		

shear, the thickness dependence of front slope stiffness is explicitly modeled by mesh. The K_s term used in the cohesive contact model was simply chosen to be very high relative to the shear stiffness of the Sylgard layer; scaling K_s in the same way as K_n results in the same neglibible effect on the front slope shearing stiffness.

It should be noted that the Sylgard debonding tests generally did exhibit some apparent rate dependence. Throughout this report the lowest tested rates have been used for calibration of the debond model. No extrapolating to the (even slower) rates of interest in our applications is proposed in the current debonding model.

The unscaled debond model parameters are summarized in Table 2. After scaling, the debond model parameters are shown in Table 3.

Table 3: Debond Model Parameters, Scaled for 20 mil Bond Thickness

	Sylgard to Aluminum	**Sylgard to PBX 9501**
K_n	49 MPa/mm	49 MPa/mm
K_s	87 MPa/mm	87 MPa/mm
τ_n	0.38 MPa	0.22 MPa
τ_s	0.18 MPa	0.17 MPa
δ_n^f	0.29 mm	0.50 mm
δ_s^f	-	0.45 mm

5 Concluding Remarks

All of the specimens described in this report consisted of two identical substrates bonded together with a thin layer of Sylgard. Post-test inspection of the failed specimens indicated that separation of the Sylgard layer generally occurred from the surface of *both* substrates in a staggered fashion - that is, some regions of Sylgard debonded from one side and stayed adhered to the other, while other regions debonded from the opposite side while staying bonded to the former side. The Sylgard did not debond from both sides of the same region until gross separation (separation much larger than the bond thickness) had occurred.

In the simulations of these tests described in the body of this report, only a single interface was allowed to separate (as illustrated in Fig. 7 and 8). Subsequent simulations, which are described and illustrated in Appendix 2, allowed both Sylgard interfaces to separate. The detailed evolution of the separation - that is, the initial location(s) and subsequent growth of the separation and the coalescence of separated regions on the interfaces of the Sylgard layer - was clearly influenced by this assumption. However, the whole-specimen load-deflection behavior was nearly identical, except at low load levels found at the end of the simulations, after the Sylgard interfaces were almost completely failed. The behavior of the progressive separation at the interface(s) is described and illustrated in Appendix 2.

Although it is more physically realistic to treat *all* Sylgard interfaces as separable, it is somewhat more computationally expensive. It is typically the case that the Sylgard layer lies between two *different* substrate materials, and it is expected that all separation will occur at the interface with the weaker damage initiation level (τ_n or τ_s). However, this situation did not exist for any of tested specimens, so there is no way to test this assumption with the current data.

Throughout this report, 2D models (plane strain for the shear specimens, axisymmetric for the cylindrical specimens) were used to investigate the behavior of the Sylgard bonded interfaces. Future investigations could use 3D models to simulate more general separation patterns, and also to investigate the role of mesh size (in the Sylgard and the substrates) in influencing the pattern of separation at the interfaces.

Future experimental investigations of Sylgard adhesive strength will make use of a different type of adhesive test and test specimen (the "blister test" investigation to be conducted by Cheng Liu, MST-8). These test results may confirm the experimental results and analytical modeling approach described in this report and reduce the considerable uncertainty in the calibration of the traction-separation model parameters developed here.

Acknowledgments

The mechanical testing of the Sylgard debond specimens was supported by programmatic funding at Los Alamos National Laboratory. Tests involving PBX 9501 were conducted by Darla Graff Thompson, Racci DeLuca, and Hongzhao Tian. Tests involving all other materials were conducted by Nickolaus Smith, Robin Pacheco, and Alyssa Reeves. Digital Image Correlation (DIC) analysis was conducted by Cheng Liu, Darla Thompson, Racci DeLuca, and Manny Lovato.

References

[1] *ABAQUS FEA*, Dassault Systemes Simulia Corporation, Providence, Rhode Island, USA.

[2] M. Afendi, *Study on Effect of Bond Thickness upon Adhesive Strength and Fracture Characteristics of Brittle Epoxy Adhesively Bonded Dissimilar Joint*, Graduate School of Systems and Information Engineering, University of Tsukuba, July 2011.

[3] K. Cho, A. Gent, *Cavitation in Model Elastomeric Composites*, Office of Naval Research, Technical Report No. 11, 1987.

[4] J. Chung, M. Chaudhury, *Soft and Hard Adhesion*, The Journal of Adhesion, 81:1119-1145, 2005.

[5] *Properties of Four Silicone Materials*, Datapoint Testing Services, December 22, 1999.

[6] A. Dorfmann, K. N. G. Fuller, R. W. Ogden, *Shear, compression, and dilatational response of rubberlike solids subject to cavitation damage*, International Journal of Solids and Structures, 39, 2002.

[7] Dow Corning Product Information sheet, *Information about Dow Corning Brand Silicone Encapsulants*, Dow Corning Corporation, Midland, Michigan.

[8] G. Flowers, B. Faubion, J. Montague, S. Switzer, *Selected Physical and Thermal Properties of Various Formulations of Silicone Potting Compounds*, Mason and Hanger-Silas Mason Co., Inc., Pantex Plant, Process Development Endeavor No. 102, November 1980.

[9] A. N. Gent, E. A. Meinecke, *Compression, Bending, and Shear of Bonded Rubber Blocks*, Polymer Engineering and Science, January 1970.

[10] J. Hoefnagels, J. Neggers, P. Timmermans, O. van der Sluis, M. Geers, *Copper-rubber interface delamination in stretchable electronics*, Scripta Materialia, 63 (2010) 875-878, 2010.

[11] I. Johnston, D. McCluskey, C. Tan, M. Tracey, *Mechanical characterization of bulk Sylgard 184 for microfluidics and microengineering*, Journal of Micromechanics and Microengineering 24 (2014) 035017.

[12] T. Kim, J. Kim, O. Jeong, *Measurement of nonlinear mechanical properties of PDMS elastomer*, Microelectronic Engineering 88 (2011).

[13] M. Lewis, R. Cohenour, T. Stephens, *Viscoelastic Properties of Three Sylgard 184 Formulations from Torsional Dynamic Modulus Testing*, Los Alamos National Laboratory report LA-UR-07-0290, November 2006.

[14] A. Lindner, T. Maevis, R. Brummer, B. Luhmann, C. Creton, *Subcritical Failure of Soft Acrylic Adhesives under Tensile Stress*, Langmuir, 20, 9156-9169, 2004.

[15] C. Liu, D. Thompson, and M. Lovato, *Bond Strength Measurement on Sylgard/Aluminum Subject to Simple Shear*, unpublished report, February 2014.

[16] Unknown author, *Dilatometer Tests on Sylgard 184: A Report on Observed CTE Values*, Los Alamos National Laboratory, MST-7 unpublished report, unknown date.

[17] B. Mukherjee, D. Dillard, R. Batra, *Numerical simulation of confinement induced instability of elastomeric layer debonding using a cohesive zone model approach*, Adhesion Society, 2014.

[18] J. Nase, A. Lindner, C. Creton, *Pattern Formation during Deformation of a Confined Viscoelastic Layer: From a Viscous Liquid to a Soft Elastic Solid*, Physical Review Letters 101, 074503 (2008), 2008.

[19] F. Schneider, T. Fellner, J. Wilde, U. Wallrabe, *Mechanical properties of silicones for MEMS*, Journal of Micromechanics and Microengineering, 18 (2008) 065008.

[20] K. R. Shull, D. Ahn, W. L. Chen, C. M. Flanigan, A. J. Crosby, *Axisymmetric adhesion tests of soft materials*, Macromolecular Chemistry and Physics, 199, 1998.

[21] N. Smith, R. Pacheco, *Sylgard Adhesive Properties*, Los Alaoms National Laboratory report W-2-TR-0042S Rev. A, 2014.

[22] B. Sorensen, T. Jacobsen, *Determination of cohesive laws by the J integral approach*, Engineering Fracture Mechanics 70 (2003) 1841-1858.

[23] F. Tanguy, M. Nicoli, A. Lindner, C. Creton, *Quantitative analysis of the debonding structure of soft adhesives*, The European Physical Journal E, 37:3, 2014.

[24] D. Thompson, R. DeLuca, H. Tian, "Summary of Shear and Tension HE Mechanical Testing, May/June 2014," unpublished report, July 2014.

[25] D. Thompson, R. DeLuca, "Summary of Sylgard Shear Stress Results," unpublished report, August 2014.

[26] A. Turon, C. Davila, P. Camanho, J. Costa, *An engineering solution for mesh size effects in the simulation of delamination using cohesive zone models*, Engineering Fracture Mechanics 74 (2007) 1165-1682, 2007.

[27] Y. Zhu, K. Liechti, K. Ravi-Chandar, *Direct extraction of rate-dependent traction-separation laws for polyurea/steel interfaces*, International Journal of Solids and Structures, 46 (2009) 31-51.

Appendix 1: Sylgard Constitutive Model

The debonding model described in this report treats the debonding process as adhesive fracture - that is, as interfacial separation between the Sylgard and one of the substrates to which the Sylgard is bonded. The behavior of the bulk Sylgard potting material itself is modeled using finite elements and a constitutive model that "know nothing" about damage, softening, or debonding. This undamaged material behavior determines the elastic response of the layer of Sylgard, and is responsible for the load-deflection behavior of the Sylgard bond test specimens before debonding damage begins. In this region the material is behaving elastically up to the point of maximum load.[13] So the first step in developing a reasonable model of the debonding behavior of the Sylgard in thin-layer applications was to consider the pre-damage load-deflection behavior.

Shear Behavior

The constitutive behavior of Sylgard 184 has been investigated by Lewis [13], who proposed a viscoelastic model appropriate for small strains and high strain rates. The tests used as the basis of Lewis' model were torsional DMA (dynamic mechanical analysis) tests conducted over a range of temperatures and cyclic frequencies. However, the strain rates of interest in the intended application of the Sylgard debonding model are very low (typically generated by diurnal temperature variations), and an appropriately long-term shear modulus was not measured in the set of tests used to calibrate Lewis' viscoelastic model.

In published articles of mechanical characterization tests of Sylgard 184 (for example, Johnston [11], Schneider [19], Kim [12]), the behavior of Sylgard 184 is nonlinear elastic, with an observed rate dependence and a material stiffening trend clearly present at strains above around 0.5. These material tests (typically uniaxial tension pull-tests using flat "ribbon" specimens) could be carried out to the point of cohesive failure with shear strains exceeding 1.0. However in the debonding tests described in this report, adhesive failure (separation at the interface of the Sylgard and substrate) occured at much lower shear stress levels than the ultimate stress exhibited in the material tests. At these lower peak stress levels, little material stiffening was observed. Therefore a linear hyperelastic material model was chosen to simulate the Sylgard behavior. A neo-hookean model gives a constant shear stiffness (that is, a linear relationship between shear stress and nominal shear strain). The shear modulus used for this model was based on the results of Johnston (G = 0.44 MPa). It is noted in the articles cited above that the elastic properties of Sylgard are influenced by factors

[13] It is emphasized that this is true in shear but not in tension; see [6].

such as cure time and cure temperature, the ratio of base resin to curing agent, and strain rate.[14]

It is noted that the apparent elastic stiffening illustrated by the ever-steepening load deflection measurements of the shear block specimens, as shown in Fig. 3 and 4, can be explained by other effects such as the nonlinear compliance of the testing machine and specimen fixture, as well as effects such as deformation of the substrates (particularly when the substrate is PBX 9501) and slight slipping of the specimen relative to the specimen holding fixtures. These effects were explored in finite element simulations of the block specimen tests. The compliance of the testing apparatus was taken into account in the simulation by including a nonlinear spring in series with the shear load, using the load-deflection measured using a surrogate all-metal specimen with no Sylgard bond. The simulations explored the effect on the load-deflection behavior due to several effects, including the clearance between the specimen and the fixture, and the coefficient of friction at the specimen / fixture interface, the thickness of the Sylgard bond layer, the role of the substrate deformation (particularly when the substrate material was PBX 9501), and the effects of mesh density. The purpose of these simulations was simply to demonstrate that the early (low force) load deflection behavior was sensitive to some of these parameters, and that very reasonble assumed values could result in a load deflection behavior that was in good agreement with the measured results.

Simulations of the shear tests were conducted to verify that the Sylgard constitutive model was capable of reproducing the undamaged (front-slope) measured load-deflection behavior. Because the front slope behavior is not influenced by debonding, the substrate material does not matter and tests using both Sylgard / aluminum specimens and Sylgard / PBX 9501 specimens could be used to characterize the load-deflection stiffness.

The result of the simulation of the tests using the shear block specimens is shown in Fig. 14. Excellent agreement in the front slope of the load-deflection curve was found except at low load levels present at the beginning of the tests. The load-deflection behavior at low load levels was strongly affected by the clearance between the block specimen and rigid fixture used to guide the shearing deformation. This clearance (which is necessary and unavoidable) allows the specimen to rotate (slightly) under the influence of the moment that is generated by the non-aligned forces on the upper and lower substrate blocks. The friction at this specimen / fixture interface also affected the early (low-force) load-deflection response.

[14] Although not employed here, a hyperelastic model can be used in conjunction with a viscoelastic treatment. The viscoelastic model proposed by Lewis could be modified with a different long-term modulus and thereby combine the advantages of a rate-dependent treatment with a nonlinear elastic response that is appropriate for large strains and long times (low strain rates).

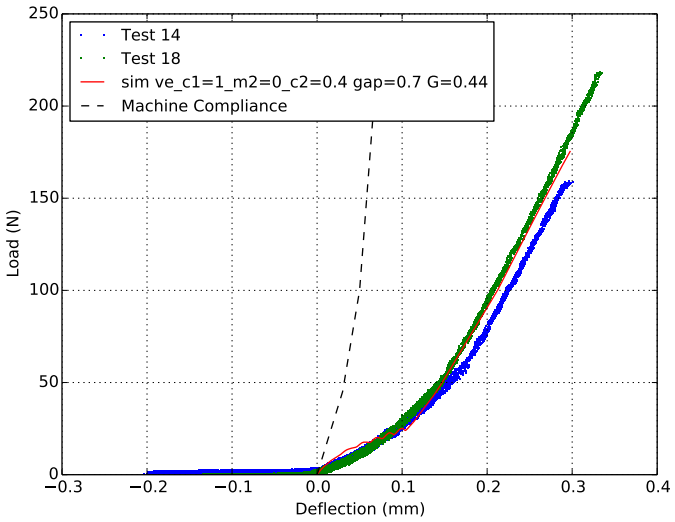

Figure 14: Comparison of the two low-rate shear block specimen tests, and the simulation of these tests. The measured machine compliance is also shown. The initial (low force) behavior of the simulation results is due to slight rotation of the specimen in the rigid fixture.

A simulation of the shear tests that used the Iosipescu specimen was also conducted. The tests that employed the optical measurement of the shear displacement were chosen because these tests gave the most accurate measurement of the shear deflection, unaffected by the compliance of testing apparatus. Having a direct measurement of the local shearing deflection also meant that no spring (representing machine compliance) was needed to simulate the front-slope loading behavior. The measurement and simulation of two of these tests is shown in Fig. 15. The Neo-Hookean elastic model did a good job of reproducing the observed load-deflection behavior, using the specimen's stated bond thickness of 2.5 mil. For comparison, a bond thickness of 3.0 mil gave even better agreement.[15]

Compressibility

The compressibility of Sylgard has been measured by an independent testing laboratory [5]. A "pressure-volume-temperature" (PVT) test was conducted in which the specific volume (volume per unit mass, which is the reciprocal of density) of a Sylgard specimen was precisely measured while varying the temperature and pressure of a surrounding liquid (mercury). From these measurements, an estimate of the

[15] It is noted that producing specimens with the intended bond thickness was unexpectedly challenging, and that there seemed to be a significant uncertainty in determining the actual thickness of the bond.

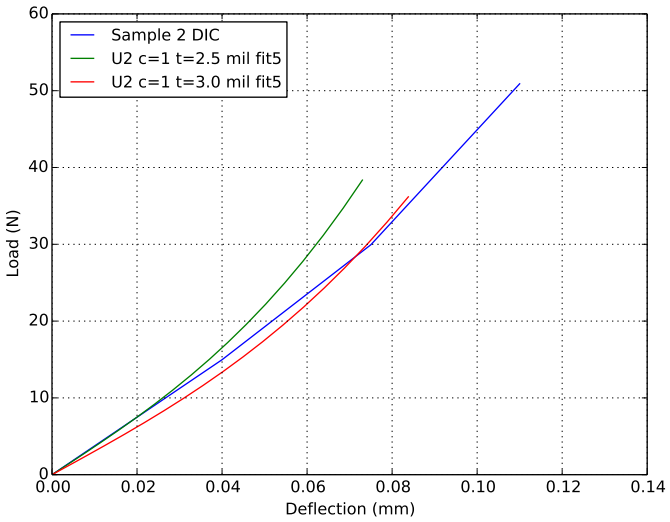

Figure 15: Comparison of the Iosipescu specimen shear response. The measured load-deflection behavior is from a test of an aluminum / Sylgard specimen, with shear deflection measured by DIC. Two bond thickness values were used in the simulation (t=2.5 mil and t=3.0 mil) for comparison.

compressive bulk modulus (at a constant temperature) and the coefficient of thermal expansion (at a constant pressure) can be calculated.

A plot of the measured pressure vs. volumetric strain (at a temperature of 33 C) is shown in Fig. 16. The volumetric strain is simply the change in specific volume (specific volume at each measured pressure, minus the specific volume at zero pressure) divided by the reference (zero pressure) specific volume:

$$e^V = \frac{V - V_0}{V_0} = \frac{V}{V_0} - 1 = J - 1 \tag{10}$$

This measure of volumetric strain is consistent with the formulation of the compressible behavior of the hyperelastic constitutive model. The pressure-strain curve was fit to a second order Ogden hyperelastic model, from which an initial (zero pressure) bulk modulus of 1,214 MPa was obtained. This value is in the range of bulk modulus values reported by Kim [12].

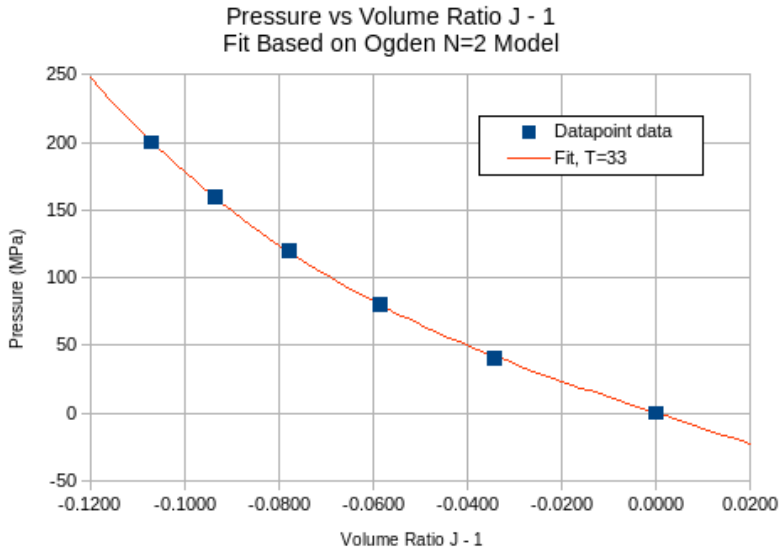

Figure 16: The pressure vs. volumetric strain behavior computed from a PVT measurement. This curve corresponds to the lowest tested temperature of 33 C.

Other Material Properties

The coefficient of thermal exansion specified by the manufacturer of Sylgard [7] is 325 microstrain/deg-K. The value calculated from the PVT data (described above) is 270 microstrain/deg-K. A third source of thermal expansion data was based on a series of dilatometer measurements [16], which obtained a value of 290.6 microstrain/K.

The density and thermal conductivity specified by the manufacturer are 1.03 g/cc and 0.16 W/m K, respectively [7]. The density measured by Datapoint Testing Services [5] is 1.024 g/cc. The specific heat capacity is reported as 0.388 cal/g C (1.624 J/g C) at a temperature of 40 C in [8].

The shear debonding tests decribed above were all conducted at room temperature (taken as 20 deg-C). The temperature dependence of the shear modulus was assumed to follow the trend measured by Schneider [19]. The normalized temperature dependence of the elastic modulus, calculated from Schneider's results, is shown in Fig. 17. Note that the modulus *increases* with increasing temperature: this is an example of the so-called "entropy spring" phenomenon. Note that the bulk modulus had the opposite temperature dependence (decreasing modulus with increasing temperature).

In summary, the Sylgard constitutive model described here was found to be capable of reproducing the load-deflection behavior observed in the Sylgard shear debonding tests, even using a coarse mesh. Table 4 summarizes all of the parameters for this

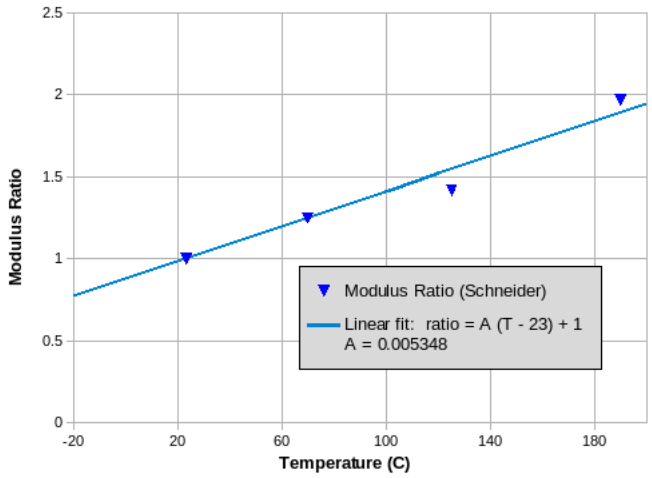

Figure 17: The temperature dependence of the normalized elastic modulus of Sylgard, based on measurements by Schneider [19]. The normalized elastic modulus is the modulus measured at each temperature, divided by the modulus measured at room temperature (T=23 C). A linear fit to this data is also shown.

Table 4: Sylgard Constitutive Model Parameters

Parameter	**Symbol**	**Value**
Initial Bulk Modulus	K_o	1214 MPa
Initial Shear Modulus	G_o	0.44 MPa
Density	ρ	1.03 g/mm3
Coefficient of Thermal Expansion	α	300e-6 1/°C
Thermal Conductivity	k	0.16 W/m °C
Specific Heat	c_p	1.624 J/g °C

model. For the thin-layer tensile debonding tests, the situation is more complicated: the state of stress and strain in a thin layer of Sylgard in a butt-tension specimen requires a fine mesh to accurately capture, but even with a very fine mesh the predicted load-deflection does not match experimental measurents. The reason for this discrepancy is thought to be due to growth of cavities (voids) originating either in the bulk or at the Sylgard/substrate interface (or both) that begins quite early (well before the peak tensile stress is reached). This phenomenon is summarized in the section on the tensile debonding model in the body of this report.

Appendix 2: Simulations of Debond Tests

The body of this report focused on the load versus extension behavior of entire Sylgard-bonded specimens, without looking more closely at the local behavior of the interface. In this appendix, the way that the Sylgard separates from one or both substrates is investigated using a series of simulations.

Two modeling approaches were considered: debonding of the Sylgard layer was assumed to occur either at a single interface, or at both interfaces simultaneously. In both cases, the load-deflection behavior of the whole specimen was found to be nearly identical until most of the load-carrying capacity was lost (that is, until well after the peak load had been developed). However, the evolution of the Sylgard/substrate separation was quite different, particularly for the tensile specimens.

Shear

The debonding separation characteristics in shear were affected by the modeling assumption of whether debonding would occur from a single Sylgard/substrate interface, or from both interfaces. Figure 18 illustrates the shear separations at the end of a simulation of the block specimen test. Shear separation has initiated from both Sylgard/block interfaces, beginning at the outer edges and progressing toward the center. A closer view of the central region of the specimen, where the transition in separation from the top and bottom blocks occurs, is shown in Fig. 19. This simulation included a small (0.7 mm, 27 mil) gap between the block specimen and one of the rigid fixtures; this gap allows a slight rotation of the specimen during loading, and also allowed the two blocks to separate (in the normal direction) after the Sylgard bonds failed. This is exactly what occurred: after the Sylgard interfaces failed, the portion of the Sylgard layer in central region tended to push the two blocks apart in the normal direction.

The whole-specimen load-deflection behavior is shown in Fig. 20. This figure shows the results for both modeling assumptions (debonding modeled at a single interface, and debonding modeled at both interfaces), as well as the measured behavior. The deflection in this plot is the crosshead deflection. The load-deflection results are nearly identical except at the end of the simulation, where the load has dropped to a small fraction of the peak load.

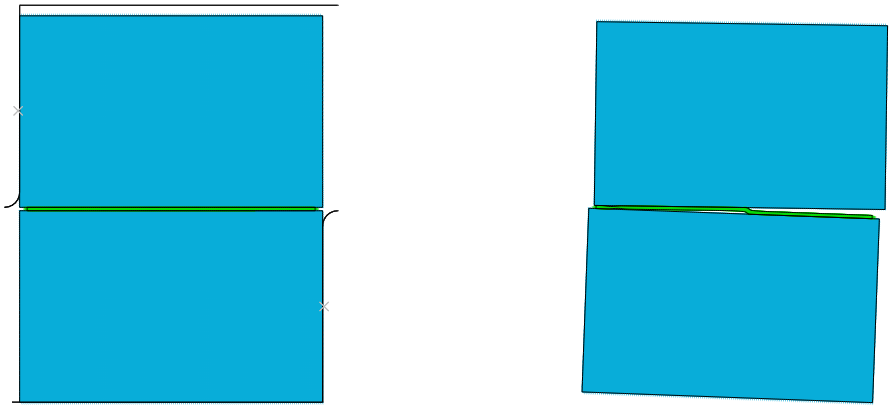

Figure 18: The initial (left) and final (right) states of the simulation of the shear test using the block specimens. Rigid fixtures (shown in the left picture) guide the shearing deformation by bearing against the bottom block (on its bottom and right sides) and the top block (on its left and top sides). A small gap between the upper block and the upper fixture allows the specimen to rotate slightly. Separaton of the Sylgard layer occurs along both of the Sylgard/block interfaces.

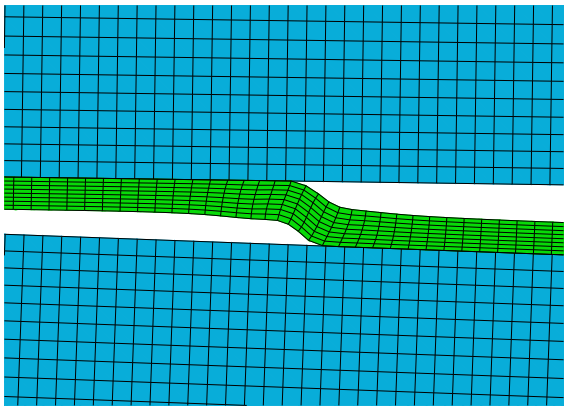

Figure 19: A close-up view of the central portion of the Sylgard layer in the shear block simulation. In this region, separation has transitioned from the top to the bottom block. After the Sylgard bonds failed, the Sylgard layer in this region tended to push the blocks apart in the normal direction.

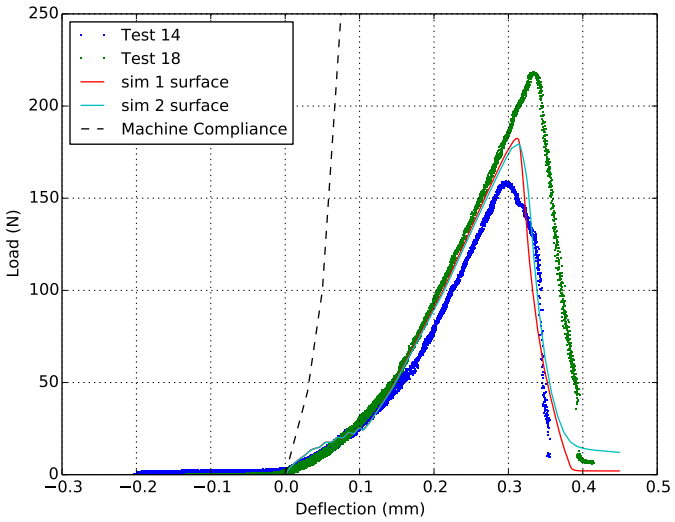

Figure 20: The load-deflection behavior from simulations of the shear block specimen. Results are shown for simulations treating debonding at a single surface only, and at both surfaces simultaneously. The load-deflection measured in these tests is also shown.

Tension

When debonding was modeled at only one Sylgard/substrate interface of the butt-tension (cylinder specimen) test, a sinusoidally-varying pattern of separation initially developed, as shown in Fig. 21. This pattern was only observed when the Sylgard mesh was very refined: for coarser meshes, the Sylgard surface separated from the substrate surface more uniformly, typically starting at the center.

When debonding was modeled at *both* Sylgard/substrate interfaces, the Sylgard initially separated in an alternating fashion between the two surfaces (the upper and lower blocks). This is illustrated in Fig. 22. During the simulation, as the block-to-block separation increased, the mode-1 (normal opening) separation evolved into a peeling mode. The simulation was not carried out long enough for complete separation, but the load had dropped to a neglibible level at the final state shown in this figure. A closer view of this alternating separation pattern is shown in Fig. 23. This alternating top/bottom separation pattern occurred for coarse and fine Sylgard meshes.

These two modeling approaches resulted in front-slope load-extension behavior that differed by a factor of two in slope (where extension was measured by the by block-to-block separation distance). The factor of two was simply due to the fact that there were two interfaces (in series), rather than a single interface. To compensate for this,

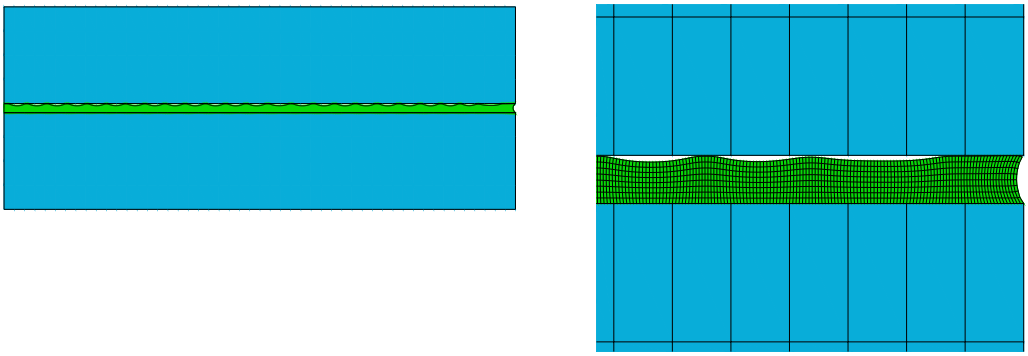

Figure 21: The separation pattern developed when only one Sylgard surface was allowed to debond in a simulation of the cylinder specimen butt-tension test. The figure on the left shows the entire model, with deformations exaggerated by a factor of 2 to help illustrate the separation pattern. The left edge of the model is the axis of of the cylinder; the right edge is the outer cylindrical surface. The figure on the right shows a closer view of the right (outer) edge of the model, with no exaggeration of deformations. At this time in the simulation, the load has dropped to a small fraction of the peak load.

the front-slope stiffness value, K_n, was doubled, resulting in nearly identical behavior. Modeling separation at one surface or at both surfaces resulted in an insignificant change in the load-extension behavior as measured by the crosshead deflection.

The post-peak (softening regime) behavior was affected by the modeling assumption of debonding at one or at both Sylgard interfaces. The pattern and evolution of the separation (illustrated above) - either intermittently separating along the single debonding interface, or alternatingly separating between the two interfaces - developed during the back slope (decreasing load) portion of the debonding process, at relatively low load levels. The whole-specimen load-deflection behavior differed very little between these two modeling approaches until the load had decreased to a fraction (roughly 25%) of its peak value. After this point, at large block-to-block separation distances, the load carrying capability was strongly affected by the single-surface vs. two-surface debonding assumption. The load-deflection results are shown in Fig. 24.

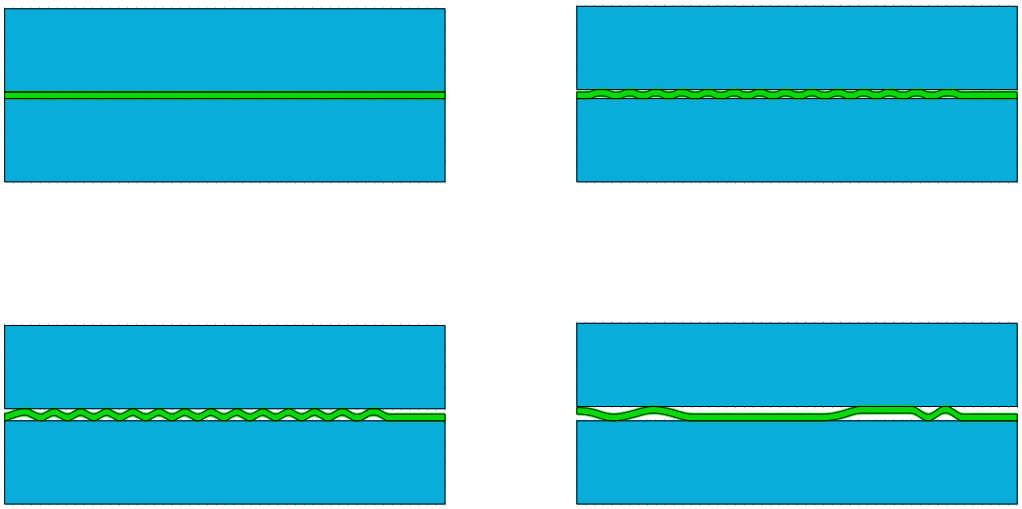

Figure 22: A series of pictures of the deformations of the Sylgard layer as the separation distance between the blocks increases. In this simulation, the Sylgard is able to debond from both blocks. The first picture corresponds to the start of the simulation of the tension test. The other pictures illustrate the separation pattern that develops during the back-slope (softening) response; the load carried by the specimen has fallen to a small fraction of the peak load by this time in the simulation.

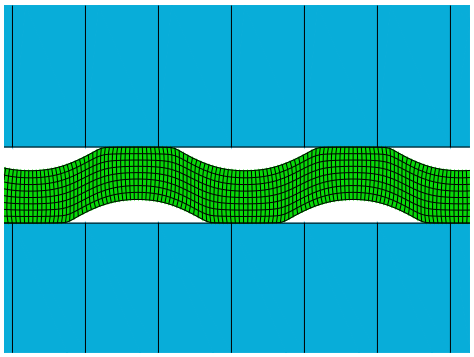

Figure 23: A closer view of the alternating separation pattern shown in the previous figure.

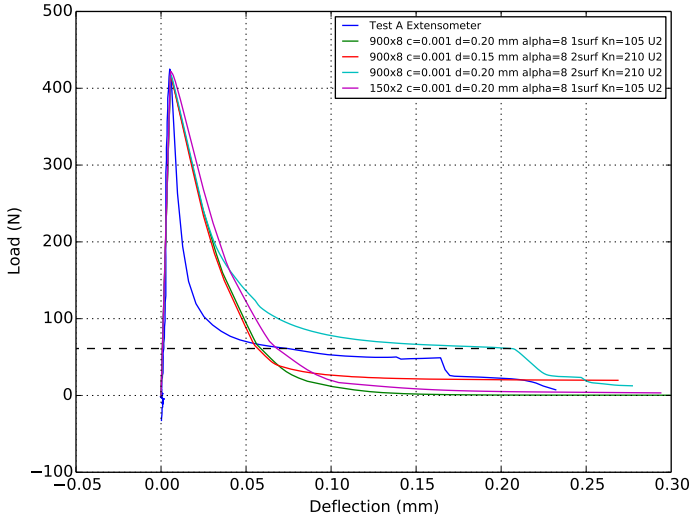

Figure 24: The load-deflection behavior from simulations of the butt-tension cylinder specimen. Results are shown for simulations treating debonding at a single surface only, and at both surfaces simultaneously. The load-deflection measured in one test of this specimen is also shown.